Lab on a Chip

TECHNICAL INNOVATION

View Article Online
View Journal | View Issue

Cite this: *Lab Chip*, 2016, **16**, 59

Controllable generation and encapsulation of alginate fibers using droplet-based microfluidics†

Chiara Martino,* Cyril Statzer, Daniele Vigolo‡ and Andrew J. deMello*

Received 24th September 2015,
Accepted 6th November 2015

DOI: 10.1039/c5lc01150g

www.rsc.org/loc

Herein we demonstrate the segmentation of alginate solution streams to generate alginate fibers of precisely controllable lengths between 200 and 1000 μm. Moreover, we demonstrate the subsequent encapsulation of the formed fibers within pL-volume microdroplets, produced within the same microfluidic device, in a direct manner. Finally, we show immediate and complete on-chip gelation of alginate fibers in a rapid and reproducible fashion.

1 Introduction

Over the last decade, the fabrication of fibrous structures on the micron scale has found numerous applications in the field of regenerative medicine[1] and tissue engineering.[2] In this regard, microfluidics has proved to be of great utility in generating chemically complex structures of tuneable geometry and in the handling of associated biomaterials.[3,4] Amongst a great variety of naturally-derived materials used for hydrogel generation in biomedical applications[5] (such as hyaluronic acid, chondroitin sulfate, chitin, chitosan, gelatin and alginate) alginate-based materials have gained particular popularity for the generation of fibrous structures.[3] Alginate is a naturally derived polysaccharide, which is soluble in aqueous solutions and undergoes gelation when exposed to cations such as Ca^{2+}.[6] Once cross-linked, alginate forms a three-dimensional (3D) elastic network with high water content, representing a favourable substrate in which to mimic the extracellular matrix (ECM) in artificial cell systems.[7] Moreover, facile gelation, the ability of this material to hold live cells (such as fibroblasts,[8] myoblasts[9] and neuronal cells[10]) and its biocompatibility, are key properties that have been widely exploited in various fields including drug delivery,[11] food formulation[12,13] and tissue engineering.[5,14]

Microfluidic systems have proved particularly advantageous in allowing the fabrication of alginate hydrogels in a rich variety of geometries. Indeed, to date, alginate spheres,[15,16] core–shell structures,[7,17,18] tear-drops,[19,20] yarn-ball geometries,[21] full fibers,[22–24] hollow fibers[25] and patterned fibers[10] have all been successfully synthesized. However, it is noted that to date no method that allows the production and *in situ* encapsulation of alginate fibers of defined length has been reported.

Alginate solutions exhibit viscoelastic shear-thinning behaviour, meaning that viscosity decreases with increasing strain rate.[26] On the molecular level, the long polymeric chains align when they are sheared and are able to slide along one another under high strain rate,[27] hence making alginate jet cutting inherently difficult. Herein, we present a strategy that allows: (i) the separation of a jet of alginate precursor solution prior to crosslinking, (ii) the immediate and complete gelation of alginate segments that prevents non-specific surface adhesion (which leads to fiber deformation and ultimately channel blockage) and (iii) the encapsulation of alginate fibers within pL-volume droplets generated within the same microfluidic device (Fig. 1).

By applying a pulsatile pressure regime to a sheathing buffer solution (defined as P_B in Fig. 1), tuned to the alginate solution viscosity, we are able to periodically cut the alginate jet (controlled by P_A). The alginate solution fragment travels into the polymerization channel where it first meets a buffer stream containing Ca^{2+} ions (Fig. 1b and c) and subsequently an oil stream (controlled by P_O in Fig. 1d) that is responsible for encapsulating the formed fibers into droplets. In contrast to prior studies that utilize a device-embedded valve for "cutting" polyethylene (glycol) diacrylate (400 Da) jets at pressures above 2 bar,[28] we are able to achieve cutting using pressures of only a few mbars, hence not affecting the downstream flows. Such an approach not only allows direct alginate segmentation but is also compatible with downstream droplet generation within the same microfluidic device. A detailed comparison between the presented approach and a lateral valve approach used for controlling polyethylene (glycol) diacrylate fiber lengths is presented in the (ESI†).

Department of Chemistry and Applied Biosciences, Institute for Chemical and Bioengineering, ETH Zurich, Vladimir Prelog Weg 1, Zürich 8093, Switzerland. E-mail: andrew.demello@chem.ethz.ch, chiara.martino@chem.ethz.ch

† Electronic supplementary information (ESI) available. See DOI: 10.1039/c5lc01150g

‡ Present address: School of Chemical Engineering, University of Birmingham, Edgbaston, Birmingham, B15 2TT, UK.

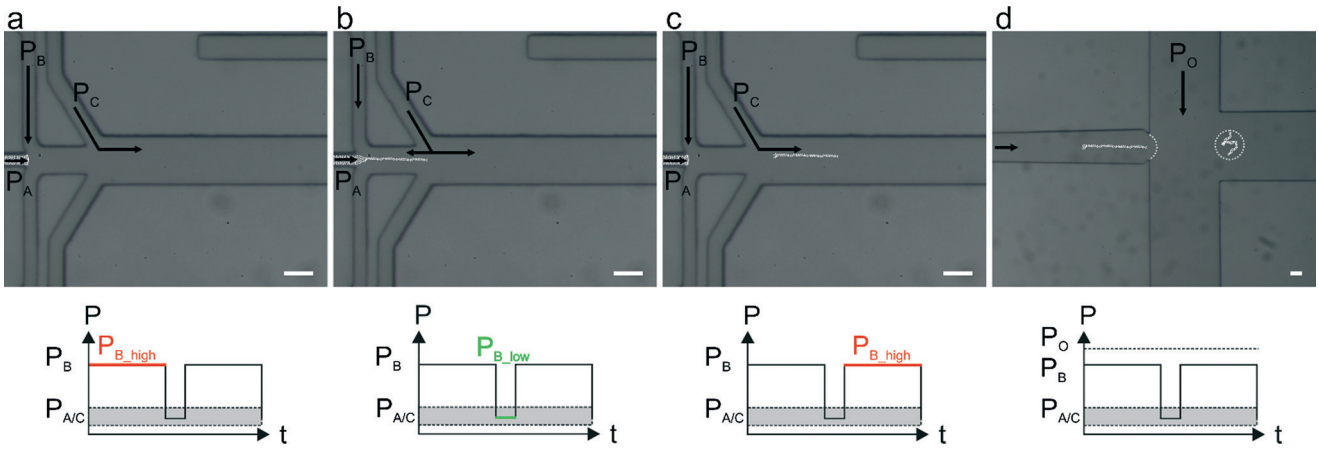

Fig. 1 Working principle for the generation and encapsulation of alginate fibers. (a–c) Optical images of the microfluidic device containing multiple inlet channels and an indication of the pressures adopted to segment an alginate input stream. Pressures of an aqueous alginate precursor solution (A), a sheathing buffer solution (B) and a buffer solution containing Ca^{2+} ions (C) are set by a pressure controller. P_A and P_C are kept constant whereas P_B follows a square wave function. Under these conditions an imposed variation in P_B (ΔP_B) causes a discontinuous flow of A and a slight backflow of C. The gelation of A occurs due to Ca^{2+} ion diffusion from the side flows and to the convective movement caused by backflow of C. (d) Optical image of the microfluidic device at the cross junction where the aqueous solutions meet an oil phase (O). The cross junction is designed to be 1 cm away from the alginate channel to ensure complete alginate polymerization prior to encapsulation. Scale bars are equal to 50 μm.

2 Experimental

Materials

A 1% (w/w) sodium alginic acid salt solution was supplemented with fluorescent beads (F8809, FluoSpheres, carboxylate-modified orange 540/560, 0.2 μm, Life Technologies, Switzerland). A 10% (w/w) dextran solution (31392 from Leuconostoc SPP, M_r 450 000–650 000, Sigma-Aldrich, Switzerland) and a 10% (w/w) dextran solution supplemented with 100 mM CaCl (Sigma-Aldrich, Switzerland) were used as sheathing and polymerizing buffers respectively. Droplets were generated using a mineral oil continuous phase (M3516, Sigma-Aldrich, Switzerland) containing 2% (w/w) Span80 (S6770, Sigma-Aldrich, Switzerland).

All solutions were regulated using a pressure controller (OB1, Elveflow, France) in combination with proprietary software (Elveflow Smart Interface, Elveflow, France). The pressure ranges for the alginate precursor solution, sheathing buffer, calcium solution and oil were 80–130 mbar, 40–190 mbar, 100–170 mbar and 200–500 mbar respectively. The lateral valve (used in control experiments) was actuated with a customised solenoid valve system (MH1, Festo, Switzerland) with applied pressures ranging from 100 to 3000 mbar.

Experimental setup

The microfluidic device design includes inlet channels for reagent delivery, a 1 cm long polymerization channel, a cross junction for droplet generation and a lateral valve (used for the control experiments described in the ESI†). Devices were produced using standard soft lithographic methods[29] in polydimethylsiloxane (PDMS). The PDMS base and curing agent (Sylgard 184, Dow Corning, USA) were mixed at a ratio of 17 : 1 (w/w), degassed and decanted onto the master. The entire structure was cured in the oven at 70 °C overnight and then peeled off the master. After punching inlet and outlet vias, the structured PDMS layer was irreversibly bonded to a clean coverglass slide (76 mm × 26 mm × 1 mm, Menzel Gläser, USA) after exposing the two surfaces to an oxygen plasma (Dieter Electronics, USA) and cured on a hot plate at 120 °C for 1 hour. To limit unwanted alginate deposition on microchannel surfaces all devices were passivated with a 1% (w/w) solution of Pluronic F-127 (P2443, Sigma-Aldrich, Switzerland) in DPBS (14190, Life Technologies, Switzerland) for 1 hour and kept at 70 °C to dry.

All optical measurements were performed using an inverted microscope (Nikon Eclipse Ti-E, Nikon, Japan) equipped with a digital camera (Orca-Flash 4.0, Hamamatsu, Japan) and a light source (LED, Prior Scientific, United Kingdom) for bright field illumination. For fluorescence measurements a mercury light source (Intensilight C-HGFI, Nikon, Japan) in combination with a Tetramethylrhodamine (TRITC) filter set (F26-516, AHF analysentechnik AG, Germany) was utilized. Images were acquired using proprietary software (HCImageLive 4.0.3.6, Hamamatsu, Japan).

Fiber lengths were calculated from fluorescence signals recorded at the cross junction (Fig. 1d), and fiber length quantification automatically processed using a script written in ImageJ 1.48v (NIH, USA). Additional details regarding analysis are provided in the ESI.†

3 Results and discussion

Synthesis of alginate fibers with different lengths

To control alginate fiber generation we explored various pulsing regimes that led to the production of fiber length ranging

from few hundreds of microns to a few millimetres. The pressures associated with the calcium chloride solution (P_C) and oil (P_O) were kept constant across all the measurements (110 mbar and 350 mbar respectively), with P_C set at a value between P_{B_low} and P_{B_high}. Moreover, the alginate solution pressure (P_A) was essentially kept constant but, according to the chosen ΔP_B for each experiment, P_A was marginally adjusted to avoid alginate backflow.

Fig. 2 illustrates representative data produced by two different pulsing regimes. In each regime, we applied an identical pulsation period and duty cycle (*i.e.* the fraction of time in which the pressure is kept high compared to the total period time) but different P_B pressure values (P_{B_low} /P_{B_high}). As shown in Fig. 2a and b, P_B followed a square wave signal with a period of 0.6 s and a 68% duty cycle, and P_B pressures were set at 90/140 mbar (Fig. 2a) and 140/160 mbar (Fig. 2b). It can be seen that variation of P_B led to a significant change in the fiber length, producing average fiber lengths of 309 ± 17 μm and 717 ± 72 μm (extracted from between 100 replicate measurements; Fig. 2c).

We also investigated the combined effect of changing the pulsation period and P_B pressure values whilst maintaining a constant duty cycle of 68%. Fig. 3a–c shows three different conditions that generate fibers of distinct lengths. In these experiments, P_B followed a square wave signal with a period of 0.4 s and values set to 70/130 mbar (Fig. 3a and condition I in Fig. 3d), a period of 0.9 s and values set to 120/160 mbar (Fig. 3b, condition II in Fig. 3d) and a period of 0.6 s and values set to 120/160 mbar (Fig. 3c, condition III in Fig. 3d). As shown in Fig. 3d, such operating conditions generated fibers with lengths ranging from approximately 200 to 1000 μm.

A more detailed summary of the variety of conditions analysed is presented in the ESI† and demonstrates that an increase in P_{B_low}, and a consequent increase of P_A, leads to a fiber length increase. Nevertheless, it is important to note that it is difficult to establish a strict relation between a single parameter and the alginate fiber length, since the experimental parameters are interdependent and cannot easily be changed in isolation. However, it is clear that the combination of a pulsatile sheathing buffer pressure and the spatial proximity of the sheathing buffer and calcium influx is essential to segment the alginate jet. Furthermore, the immediate calcium exposure favours fiber gelation over the re-joining of two consecutive un-polymerised alginate segments, with the backflow of Ca^{2+} ions in the buffer channel guaranteeing fast gelation of each alginate segment.

Synthesis of patterned alginate fibers

As previously noted, a mild backflow of Ca^{2+} ions in the sheathing buffer channel accelerates alginate polymerization without causing alginate deposition. However, if P_A is increased and the lower buffer pressure (P_{B_low}) decreased, the precursor alginate solution is able to flow into the sheathing buffer channel where it polymerizes leaving an imprint on the alginate fiber. Fig. 4a–f shows a time sequence of a single cycle whilst Fig. 4g shows an alginate fiber containing repetitive units obtained from channel imprinting after two cycles. Fibers were generated with P_A = 129 mbar, P_B = 40/160 mbar and a period and duty cycle equal to 0.6 s and 68% respectively.

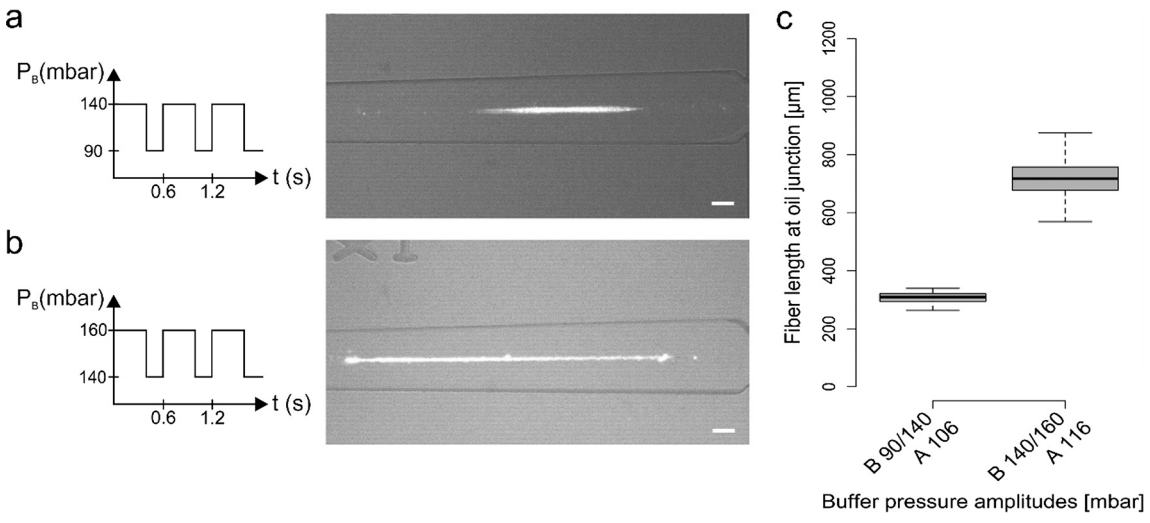

Fig. 2 Generation of alginate fibers using a constant P_B pulsation period and different P_B pressure values. (a–b) Two operating conditions, which differ in P_{B_low}/P_{B_high} values and alginate pressure, produce different fiber lengths at the end of the polymerization channel. In both experiments the duty cycle and pulsation period are equal to 68% and 0.6 s respectively. (c) Box plot of fiber lengths obtained at P_B = 90/140 mbar, P_A = 106 mbar and P_B = 140/160 mbar, P_A = 116 mbar showing two distinct fiber populations with average lengths equal to 309 ± 17 μm and 717 ± 72 μm respectively. Scale bars are equal to 50 μm.

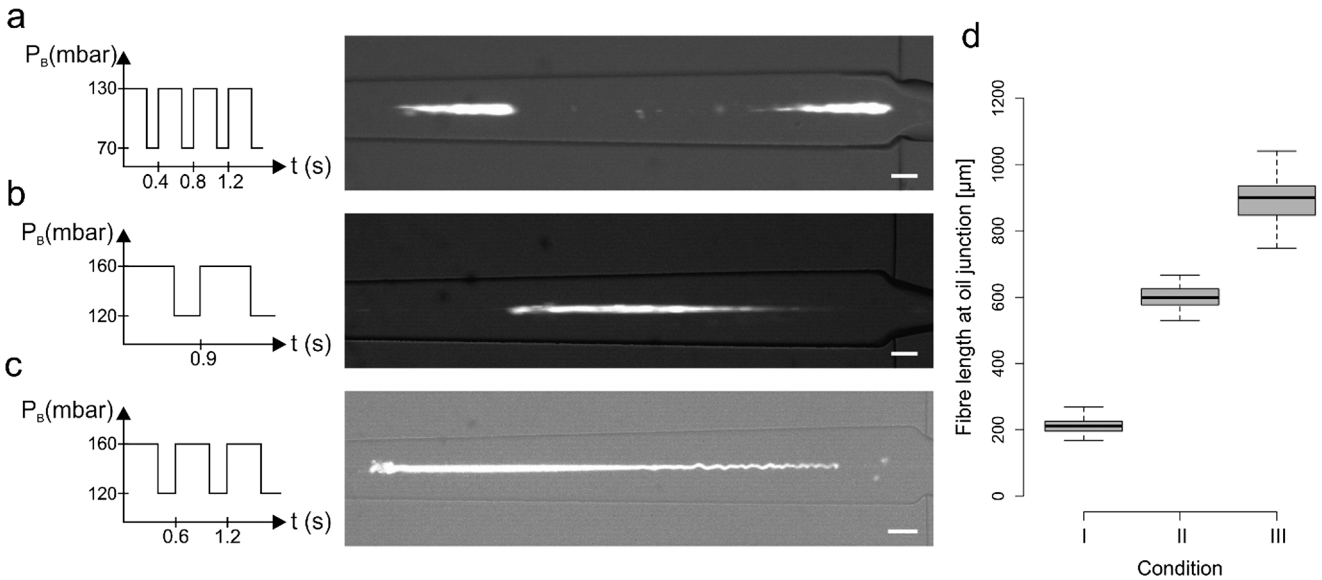

Fig. 3 Generation of alginate fibers using different P_B pulsation periods and different P_B pressures. (a–c) Three operating conditions, which differ in pulsation period, P_{B_low}/P_{B_high} and alginate pressures, produce different fiber lengths at the end of the polymerization channel. For all conditions the duty cycle is equal to 68%. (d) Box plot of fiber lengths at three different conditions shows alginate fiber lengths of 218 ± 21 μm (condition I), 598 ± 33 μm (condition II) and 900 ± 106 μm (condition III). Condition I: P_A = 102 mbar and P_B = 70/130 mbar with a period equal to 0.4 s. Condition II: P_A = 115 mbar and P_B = 120/160 mbar with a period equal to 0.9 s. Condition III: P_A = 115 mbar and P_B = 120/160 mbar with a period of 0.6 s. Scale bars are equal to 50 μm.

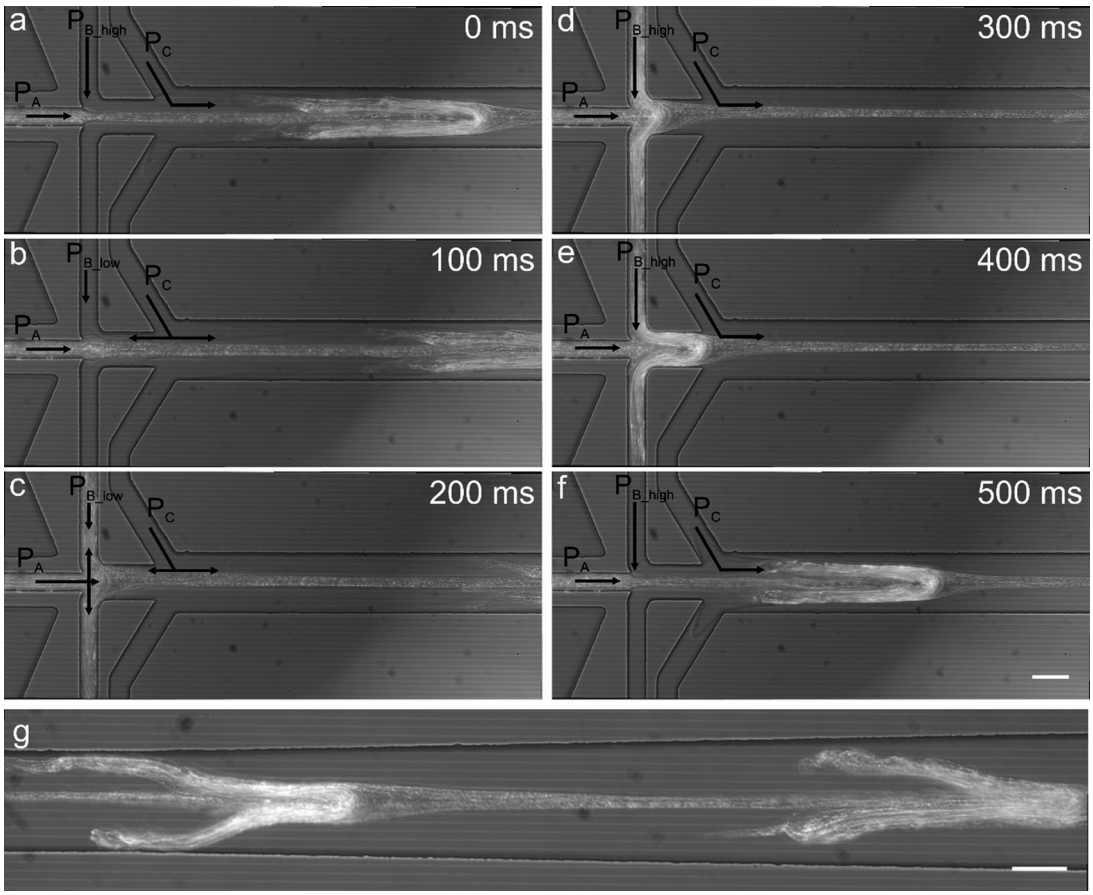

Fig. 4 Generation of regularly patterned alginate fibers. A variation of the operating conditions imposed in Fig. 2b leads to the production of a continuous alginate fiber displaying regular dispersed protrusions. This is achieved by increasing ΔP_B and increasing the alginate pressure. Starting from the pressure conditions in Fig. 2b, by decreasing the P_{B_low} to 40 mbar and increasing the alginate pressure to 129 mbar the alginate solution and Ca^{2+} ions flow into the sheathing buffer channel and initiate gelation (a–c); as soon as the P_B becomes higher, the polymerised alginate is pushed out forming a fiber containing imprinted features (d–f) which flows downstream (g). Scale bars are equal to 50 μm.

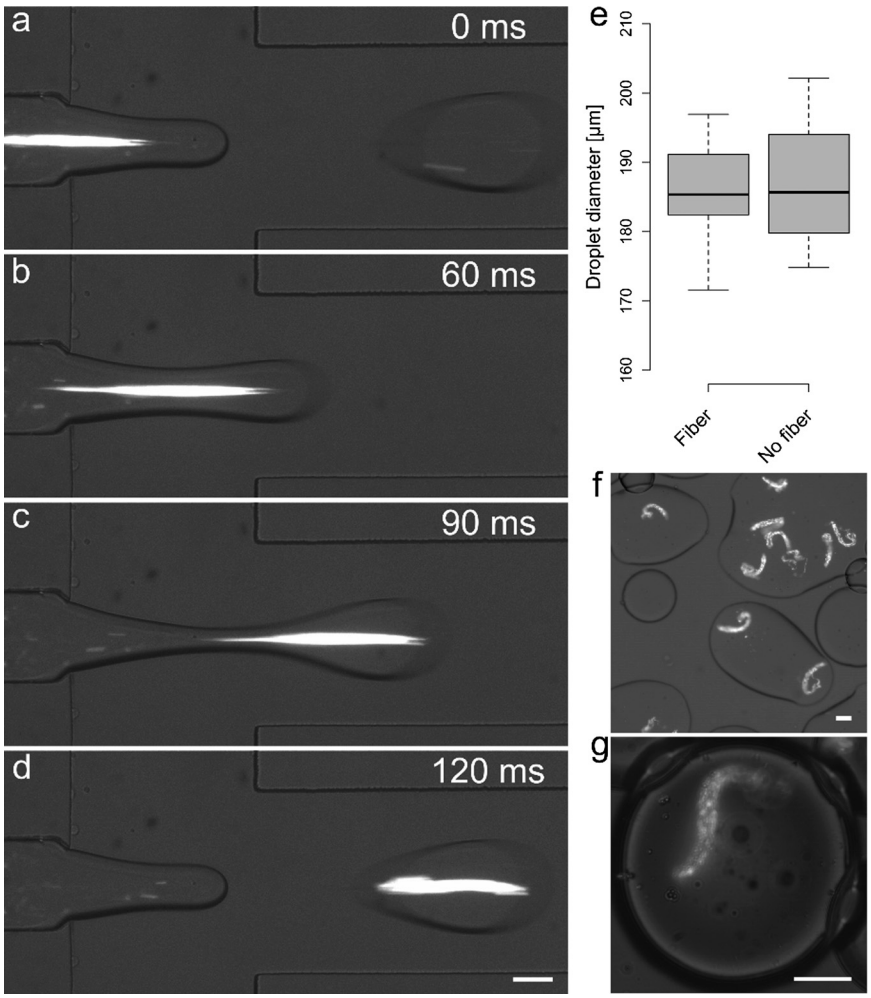

Fig. 5 Fiber encapsulation. (a–d) Encapsulation of a single alginate fiber into a microdroplet occurring at the end of the polymerizing channel. Fibers were produced by setting P_A = 109 mbar, P_B = 100/160 mbar with period equal to 0.4 s and 50% duty cycle and P_c = 110 mbar. (e) Box plot showing the diameters of filled (186 ± 7 μm) and empty droplets (187 ± 8 μm) generated using P_O = 350 mbar. (f) Droplets collected outside the device and smeared on a coverglass slide, showing no change in fiber shape. (g) A representative droplet-encapsulated alginate fiber collected off chip 1 hour after generation, illustrating complete gelation and no significant shape change. Scale bars are equal to 50 μm.

Fiber encapsulation

Alginate fibers generated by using P_A = 109 mbar and P_B = 100/160 mbar with period equal to 0.4 s, a 50% duty cycle and P_c = 110 mbar could be directly encapsulated into pL-volume droplets. P_O was set to 350 mbar and droplets of an average diameter of 186 μm (C.V. = 5%) were produced at a frequency of 8.4 Hz. Fig. 5a–d shows representative time frames during the encapsulation of a 300 μm long alginate fiber. Under the current operating conditions one out of three droplets could be loaded with an *in situ* generated fiber. As shown in Fig. 5e, the fiber encapsulation process does not affect droplet diameter. Moreover, small variations in oil pressure (±10%) did not affect upstream fiber generation, thus allowing control over both droplet size and fiber encapsulation. To ascertain whether gelation of the alginate fiber occurred within the device, a drop (100 μL) of the emulsion produced on-chip was deposited and smeared onto a coverglass slide (Fig. 5f). No significant deformation in fiber shape could be observed and imaging of droplets containing alginate fibers 1 hour after generation confirmed that alginate fiber shape was identical to that observed during encapsulation (Fig. 5g).

Fouling

Fouling is a common problem encountered in microfluidic devices, especially when directly bonded on glass surfaces since glass has a very high nonspecific binding capacity for proteins and other biomolecules.[30] A number of methods have been developed to limit this problem.[31] In this work, surface treatment with Pluronic-127 was successful in preventing fouling when compared to uncoated devices. The time until the first alginate deposition occurred increased from approximately 1 minute, in uncoated devices, to between 5 and 10 minutes when coated with Pluronic-127. Furthermore, fouling on the coated surface displayed a much weaker attachment and, thus could be removed immediately

by the next fiber. We also observed that this "self-cleaning" effect was more efficient when the diameter of the polymerization channel was smaller, since the fiber was less likely to pass around the attached fibers. If such a self-cleaning process proved ineffective, an increase in alginate pressure for two seconds was used to purge the polymerization channel, giving the devices a working lifetime of up to 60 minutes.

4 Conclusions

In this work, we present a new microfluidic strategy to segment an alginate precursor solution and generate alginate fibers. The combined effects of pulsatile pressure control and immediate exposure to a buffer solution containing Ca^{2+} ions are responsible for the generation of alginate fibers of different lengths, ranging from a few hundreds of microns to up to one millimetre. Alginate fibers of different length are of potential utility in culturing small cell populations in spatially defined environments and in a high-throughput manner, thus enabling hydrogel-shape dependent studies of cellular behaviour (as well as unlocking potential applications in biofabrication). Our approach is highly successful in achieving fast alginate gelation over very short distances, which in turn allows the encapsulation of polymerised fibers within the same microfluidic device. This feature will be particularly interesting in droplet-based application, for example for the generation of artificial cell constructs[32,33] containing inner scaffolding. In this way it is possible to generate systems that can mimic functions of cells like the presence of a membrane setting a boundary of an inner compartment of controlled and well defined geometry. We can predict that the construction of such entities not only will offer the possibility of replacing faulty biological components in individuals affected by severe pathologies, as it is already happening for microfabricated tissue engineering products,[3] but will also facilitate the understanding of components of life by making from scratch.

Acknowledgements

Chiara Martino acknowledges support from the ETH Zurich Postdoctoral Fellowship Program and Marie Curie Actions for People COFUND Program.

References

1 H. Onoe and S. Takeuchi, *Drug Discovery Today*, 2015, **20**, 236–246.
2 A. Tamayol, M. Akbari, N. Annabi, A. Paul, A. Khademhosseini and D. Juncker, *Biotechnol. Adv.*, 2013, **31**, 669–687.
3 M. A. Daniele, D. A. Boyd, A. A. Adams and F. S. Ligler, *Adv. Healthcare Mater.*, 2015, **4**, 2–2.
4 K. Ren, Y. Chen and H. Wu, *Curr. Opin. Biotechnol.*, 2014, **25**, 78–85.
5 B. G. Chung, K.-H. Lee, A. Khademhosseini and S.-H. Lee, *Lab Chip*, 2012, **12**, 45–59.
6 I. Machida-Sano, M. Hirakawa, H. Matsumoto, M. Kamada, S. Ogawa, N. Satoh and H. Namiki, *Biomed. Mater.*, 2014, **9**, 025007.
7 C. Martino, T. Y. Lee, S.-H. Kim and A. J. deMello, *Biomicrofluidics*, 2015, **9**, 024101.
8 K. Y. Lee, E. Alsberg, S. Hsiong, W. Comisar, J. Linderman, R. Ziff and D. Mooney, *Nano Lett.*, 2004, **4**, 1501–1506.
9 E. Alsberg, K. W. Anderson, A. Albeiruti, R. T. Franceschi and D. J. Mooney, *J. Dent. Res.*, 2001, **80**, 2025–2029.
10 Y. Kitagawa, Y. Naganuma, Y. Yajima, M. Yamada and M. Seki, *Biofabrication*, 2014, **6**, 035011.
11 T. W. Wong, *J. Pharm. Pharmacol.*, 2011, **63**, 1497–1512.
12 L. H. Pignolet, A. S. Waldman, L. Schechinger, G. Govindarajoo, J. S. Nowick and L. Ted, *J. Chem. Educ.*, 1998, **75**, 1430.
13 A. Escarpa, *Lab Chip*, 2014, **14**, 3213–3224.
14 K. Y. Lee and D. J. Mooney, *Prog. Polym. Sci.*, 2012, **37**, 106–126.
15 S. Sugaya, M. Yamada, A. Hori and M. Seki, *Biomicrofluidics*, 2013, **7**, 054120.
16 W. H. Tan and S. Takeuchi, *Adv. Mater.*, 2007, **19**, 2696–2701.
17 P.-W. Ren, X.-J. Ju, R. Xie and L.-Y. Chu, *J. Colloid Interface Sci.*, 2010, **343**, 392–395.
18 J. Wu, T. Kong, K. W. K. Yeung, H. C. Shum, K. M. C. Cheung, L. Wang and M. K. T. To, *Acta Biomater.*, 2013, **9**, 7410–7419.
19 C. J. Martinez, J. W. Kim, C. Ye, I. Ortiz, A. C. Rowat, M. Marquez and D. Weitz, *Macromol. Biosci.*, 2012, **12**, 946–951.
20 Y. Hu, G. Azadi and A. M. Ardekani, *Carbohydr. Polym.*, 2015, **120**, 38–45.
21 A. Miyama, M. Yamada, S. Sugaya and M. Seki, *RSC Adv.*, 2013, **3**, 12299–12306.
22 M. Yamada, S. Sugaya, Y. Naganuma and M. Seki, *Soft Matter*, 2012, **8**, 3122–3130.
23 E. Kang, S.-J. Shin, K. H. Lee and S.-H. Lee, *Lab Chip*, 2010, **10**, 1856–1861.
24 S.-J. Shin, J.-Y. Park, J.-Y. Lee, H. Park, Y.-D. Park, K.-B. Lee, C.-M. Whang and S.-H. Lee, *Langmuir*, 2007, **23**, 9104–9108.
25 K. H. Lee, S. J. Shin, Y. Park and S.-H. Lee, *Small*, 2009, **5**, 1264–1268.
26 R. A. Rezende, P. J. Bártolo, A. Mendes and R. M. Filho, *J. Appl. Polym. Sci.*, 2009, **113**, 3866–3871.
27 K. Brian, *Micro- and Nanoscale Fluid Mechanics Transport in Microfluidic Devices*, Cambridge University Press, 2009.
28 J. K. Nunes, K. Sadlej, J. I. Tam and H. A. Stone, *Lab Chip*, 2012, **12**, 2301–2304.
29 Y. N. Xia and G. M. Whitesides, *Angew. Chem., Int. Ed.*, 1998, **37**, 550–575.
30 P. K. Sorger, *Nat. Biotechnol.*, 2008, **26**, 1345–1346.
31 I. Banerjee, R. C. Pangule and R. S. Kane, *Adv. Mater.*, 2011, **23**, 690–718.
32 C. Martino, L. Horsfall, Y. Chen, M. Chanasakulniyom, D. Paterson, A. Brunet, S. Rosser, Y.-J. Yuan and J. M. Cooper, *ChemBioChem*, 2012, **13**, 792–795.
33 C. Martino, S.-H. Kim, L. Horsfall, A. Abbaspourrad, S. J. Rosser, J. Cooper and D. A. Weitz, *Angew. Chem., Int. Ed.*, 2012, **51**, 6416–6420.

